

Photon-photon quantum phase gate in a photonic molecule with $\chi^{(2)}$ nonlinearity

Ming Li,^{1,2} Yan-Lei Zhang,^{1,2} Hong X. Tang,³ Chun-Hua Dong,^{1,2,*} Guang-Can Guo,^{1,2} and Chang-Ling Zou^{1,2,4,†}

¹Key Laboratory of Quantum Information, Chinese Academy of Sciences,
University of Science and Technology of China, Hefei 230026, P. R. China.

²CAS Center For Excellence in Quantum Information and Quantum Physics,

University of Science and Technology of China, Hefei, Anhui 230026, P. R. China.

³Department of Electrical Engineering, Yale University, New Haven, CT 06511, USA

⁴National Laboratory of Solid State Microstructures, Nanjing University, Nanjing 210093, China.

(Dated: February 19, 2024)

The construction of photon-photon quantum phase gate based on photonic nonlinearity has long been a fundamental issue, which is vital for deterministic and scalable photonic quantum information processing. It requires not only strong nonlinear interaction at the single-photon level, but also suppressed phase noise and spectral entanglement for high gate fidelity. In this paper, we propose that high-quality factor microcavity with strong $\chi^{(2)}$ nonlinearity can be quantized to anharmonic energy levels and be effectively treated as an artificial atom. Such artificial atom has a size much larger than the photon wavelength, which enables passive and active ultra-strong coupling to traveling photons. High-fidelity quantum control-phase gate is realized by mediating the phase between photons with an intermediate artificial atom in a photonic molecule structure. The scheme avoids the two-photon emission and thus eliminates the spectral entanglement and quantum phase noises. Experimental realization of the artificial atom can be envisioned on the integrated photonic chip and holds great potential for single-emitter-free, room-temperature quantum information processing.

Introduction.- Quantum photonic integrated circuit (PIC) has been extensively studied since the last decade for photon-based quantum information processing [1–5], due to its advantages of stability, compactness and low power consumption. Essential quantum optical components, including quantum photon sources [6], quantum gates [7, 8] and single-photon detectors [9–11], have been all demonstrated on the PIC with excellent performances, and fully integrated quantum PIC is within reach [12]. However, the absence of single-photon nonlinearity greatly limits the development of PIC for scalable quantum processors [13], since the deterministic quantum gates among photons are forbidden. For example, a photon-photon quantum phase gate requires the controlling of the phase of one photon by another photon [14]. It is believed that the intrinsic nonlinear effect of a dielectric is too weak compared with the material absorption [13], thus the desired quantum operation can not be accomplished before the photon is lost. As a result, the photonic two-qubit quantum gates are implemented probabilistically with pure linear optical components and rely on quantum interference and ancillary photons [7, 15]. Another approach to overcome this obstacle is introducing single emitters into the PIC, while suffering from the experimental challenges of nano-manipulation and instabilities of emitters [16–18].

Fortunately, recent exciting progress in nonlinear optics on PIC has encouraged the efforts to pursue nonlinearity at the single-photon level, with the help of sophisticated fabrication technique, new material, and advanced photonic structure engineering. By realizing the micro- and nano-resonators of ultrahigh quality factor and ultrasmall mode volume, the cavity photonic nonlinear interaction strength is greatly boosted while the losses are suppressed [19–22]. In the past few years, cavity-enhanced nonlinear photonics has achieved great success in frequency conversion, frequency comb, and quantum

photon sources [20, 23–26]. Especially, ultrahigh-efficiency second-harmonic generation (SHG) with efficiency as high as $10^3 - 10^6 \%$ /W are achieved [27–30]. All these exciting progresses achieved with $\chi^{(2)}$, such as in lithium niobate (LN) [30–33], aluminum nitride (AlN) [27, 34] and gallium arsenide (GaAs) [28] indicate a saturation of conversion efficiency even at single-photon level pump, and reveal a promising path towards single-photon nonlinearity.

However, there is still another obstacle for the deterministic photonic quantum gates, since they demand the processing of photon's quantum states while maintaining their spectral-temporal wavefunction. As pointed out by Shapiro [35–37], the fidelity of photon-photon quantum gate based on photonic nonlinearity, such as Kerr effect, suffers from spectral entanglement and phase noise, due to the spatially-local interaction and multimode nature of traveling photons in the frequency domain. Even though several schemes have been proposed to overcome such limitation by introducing non-local interaction and cascaded sites [38–40], these works are still based on propagation modes and the optical loss in nonlinear media is not considered. Besides, the Kerr nonlinearity is mediated by neutral atoms, which has finite linewidth and its integration with the photonic chip is challenging in practice.

In this work, we propose an artificial atom on PIC by utilizing $\chi^{(2)}$ nonlinearity in a well-engineered microresonator. The artificial atom has a size of microns, and is thus easy for fabrication and is scalable. Compared with neutral atoms, the artificial atoms can strongly couple with a waveguide, so the photon could be stored and extracted efficiently. Additionally, the artificial atom possesses degenerate chiral energy levels, so allowing for mediating unidirectional photon-photon interactions. As an example, we proposed an architecture for realizing quantum control-Z (CZ) gate based on a photonic molecule [32]. By treating one of the resonators as a tun-

able antenna for coupling the photons with the other artificial atom, the single photons can be stored and coupled with each other strongly, breaking the limitations of the spatially local interaction condition for traveling photons, thus being immune from spectral entanglement and phase noises. With potentially achievable parameters in the experiment, we predict a fidelity of CZ gate of 99%. Combining with the mature single-qubit gates (Hadamard and phase gates) by linear optical elements, the universal gate sets [14] could be accomplished and the scalable quantum computation is promising on the PIC platform.

Artificial atom.— Figure 1(a) schematically illustrates the artificial atom, which is based on phase-matched $\chi^{(2)}$ ultrahigh-Q microresonator. In the view of nonlinearly coupled optical modes, the system Hamiltonian reads [24, 27] ($\hbar = 1$)

$$H_{AA} = \sum_j \omega_j j^\dagger j + g_d (a^{\dagger 2} c + a^2 c^\dagger), \quad (1)$$

with $j \in \{a, c\}$ and the mode frequency $2\omega_a \approx \omega_c$ for degenerate three-wave mixing process. For the non-degenerate case $j \in \{a, b, c\}$, the interaction reads $g_{nd} (a^\dagger b^\dagger c + abc^\dagger)$ with $\omega_a \neq \omega_b$ and $\omega_b \approx \omega_c - \omega_a$. Here, a, b, c denotes the bosonic operator for the modes, and $g_{d,nd} \propto \chi^{(2)} \xi / \sqrt{V}$ is the coupling strength which is determined by the modal overlap ξ , cavity mode volume V , and the material nonlinear susceptibility $\chi^{(2)}$.

In conventional bulk nonlinear optics, the coupling rate is much weaker than the dissipation rate ($g \ll \kappa$) due to large V , thus the conversion from a, b to c only occurs by strongly pumping the system [24, 27]. With improved ξ and drastically reduced V in PIC, g increases and approaches κ , and thereby the quantum effect appears, as shown by the right panel of Fig. 1(a). Considering only few excitations in those modes, the system energy levels can be rewritten as $|l_a n_c\rangle$ or $|l_a m_b n_c\rangle$ by Fock state basis, with $l, m, n \in \mathbb{Z}$ (the subscripts of the states are omitted in the following). Due to the nonlinear interaction in degenerate case, the energy levels $|20\rangle$ and $|01\rangle$ are hybridized and produce eigenstates $(|20\rangle \pm |01\rangle) / \sqrt{2}$, whose energy levels shifted by $\pm \sqrt{2}g_d$, respectively. Similarly, for the non-degenerate case, the state $|110\rangle$ strongly couples with $|001\rangle$ and produces new eigenstates $(|110\rangle \pm |001\rangle) / \sqrt{2}$ with a frequency splitting $2g_{nd}$. Then, the cavity shows anharmonicity for Fock states of modes a (or a and b), as shown by the dashed lines in Fig. 1(a). When $\kappa < g_{d,nd}$, the second photon can not enter into the cavity if mode a is already occupied by one single-photon, which would lead to the photon-blockade effect [41–43]. In this case, we treat the cavity as an artificial atom. It is worth noting that, the artificial atom based on the anharmonicity of Fock states shares the same spirit of superconducting qubit [44], which is an LC circuit with strong anharmonicity and is usually treated as a two-level system.

To verify the artificial atom, a weak coherent driving $\epsilon_p (a^\dagger + a)$ is used to probe the system with $g_d/\kappa_a = 4$ and $g_d/\kappa_a = 4$ for the degenerate case. Figure 1(b) shows the dependence of the $|20\rangle$ state population on the frequency of a continuous driving field ($\epsilon_p = 0.2$). The population at zero de-

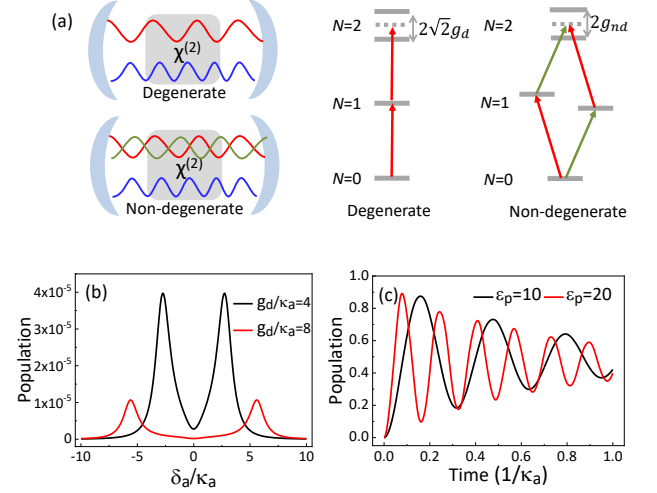


FIG. 1. Artificial atom based on an optical cavity with strong $\chi^{(2)}$ nonlinearity. (a) Left: schematic of degenerate and non-degenerate three-wave mixing, corresponding to second-harmonic generation (SHG) and sum-frequency generation (SFG). Right: energy level structures for $\chi^{(2)}$ interaction. The energy levels of two-excitation state split by $2\sqrt{2}g_d$ for degenerate case and $2g_{nd}$ for non-degenerate case due to $\chi^{(2)}$ interaction. (b) Vacuum Rabi splitting of the populations of state $|2a0c\rangle$ for SHG in the cavity. The coupling strengths are set $g_d/\kappa_a = 4$ for the black curve and $g_d/\kappa_a = 8$ for the red curve. The driving strength is $\epsilon_p = 0.2$. The Rabi splitting is proportional to the nonlinear coupling strength. (c) Rabi oscillation of the single-photon excitation state $|1a0c\rangle$ population under coherent driving. The coupling strength is $g_d/\kappa_a = 80$ and the driving strength is $\epsilon_p = 10$ for the black curve $\epsilon_p = 20$ for the red curve. The cavity decay rates of the fundamental and second-harmonic modes are set $\kappa_a = \kappa_c = 1$.

tunings is greatly suppressed due to the splitting of the hybrid energy levels. Furthermore, the temporal behavior of the artificial atom under the on-resonance driving shows clear Rabi oscillation [Fig. 1(c)], since only $|00\rangle$ and $|10\rangle$ can be effectively excited, thus confirms the equivalence of our system to a two-level atom. The blockade effect to the high-excitation energy levels can be used to build a deterministic single-photon source.

Compared with natural atoms, the artificial atom maintains many advantages of photonic cavities. Firstly, degenerate clockwise (CW) and counter-clockwise (CCW) modes are supported in a traveling wave microresonator. Therefore, the artificial atom can couple with external photons unidirectionally [Fig. 2(a)], which is only possible for natural atoms with photonic spin-orbital coupling [45]. Especially, the two-fold degeneracy of modes enables the construction of two identical artificial atoms with only one design, offering more energy levels for quantum information processing. Secondly, the artificial atoms are more flexible for photonic structure designs and allow highly efficient coupling with a waveguide or other photonic structures. For studying waveguide quantum electrodynamics [46], the artificial atom to waveguide coupling can achieve a Purcell factor F_p exceeding 1000 [with the configu-

ration in Fig. 2(a)]. In contrast, the achievable F_p for natural atom-waveguide coupling is limited to $\mathcal{O}(1)$. In addition to the passive design, the interaction between the artificial atom and photons could also be dynamically controlled by active antennas [Fig. 2(b)]. The energy levels of artificial atoms are also reconfigurable, as the resonance frequencies can be dynamically tuned by external drive fields via the electro-optic (EO) or thermal-optic effects.

CZ gate.— These merits of artificial atoms make it an excellent platform for realizing scalable quantum gates for photons or atoms. Employing the photon blockade effect in strongly coupled artificial atom and waveguide, the probe single photon would gain a π phase when passing the artificial atom if its frequency is on-resonance with its transition [see the Supporting Materials (SM) for details]. However, if the photon is off-resonance with the transition, the artificial atom would not induce a phase shift. Therefore, it is anticipated that one photon could induce a π -phase shift of another photon, manifesting the CZ gate for photons. We numerically tested the artificial atom by coupling it to a bus waveguide [Fig. 2(a)] with an input of two cooperating photons [Fig. 2(c)]. The outcome [Fig. 2(d)] shows a broadened spectrum distribution and undesired frequency correlation between the two photons. The output is a superposition of the directly transmitted state and the two-photon bound state [47–49], which means the frequency of the output photons are entangled. Therefore, it is failed to obtain the CZ gate because the artificial atom not only induces a π -phase change but also induces the entanglement of other degree of freedom. Such a problem has also been predicted in previous Kerr-type nonlinear medium [38, 40], and the reason should be attributed to the continuum modes in the waveguide: the excitation states $|01\rangle$ and $|20\rangle$ of artificial atom could spontaneously emit photon pairs without conserving the frequency of individual photons, although the total energy of two photons conserves.

The direct two-photon interaction mediated by the artificial atom prevents building a quantum logic gate. In other words, the two-photon spontaneous emission channels of the artificial atom must be suppressed during the gate operation, thus the coupling between the continuum and the energy levels of the artificial atom for either control or target photon should be shut-off. Therefore, we introduce a scheme based on storing the control photon in the artificial atom, to avoid the decay of control photon level to the continuum during its interaction with the target photon, and realize a photon-photon quantum phase gate on PIC.

As shown in Fig. 3(a), an architecture based on the photonic molecule is proposed to perform the CZ gate. The architecture composed of two microresonators and a bus waveguide, with one microresonator engineered for artificial atom, while the other served as an antenna to simultaneously couple with the artificial atom and waveguide [Fig. 2(b)]. Since the two microresonators are made with the same $\chi^{(2)}$ material, thus the frequency of the antenna could be modulated by EO effect and thereby the coupling between the waveguide and artificial atom could be controlled in real-time. Such a

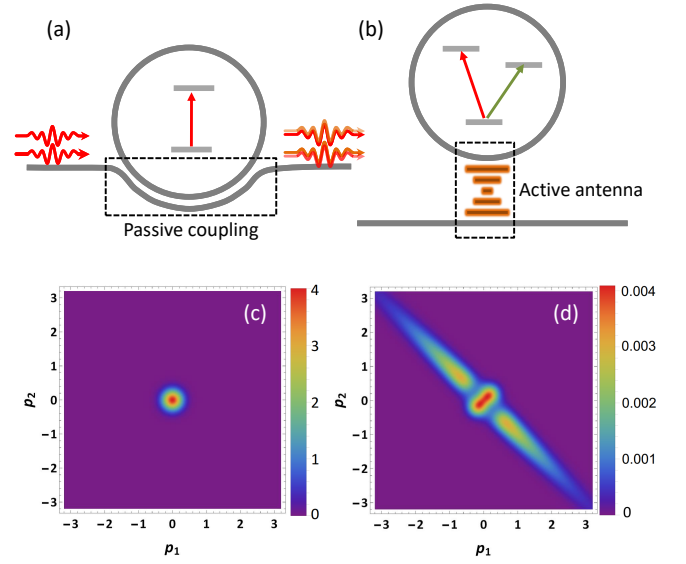


FIG. 2. Passive and active coupling between waveguide and artificial atom made by microring cavity. (a)-(b) The photonic designs for the coupling between waveguide and artificial atom. (a) The artificial atom is coupled with a waveguide of wrapped-around structure. The coupling rate can be three orders of magnitude than the decay rate. (b) The atom-waveguide coupling is dynamically controlled by an active antenna. Photons of different pulse shapes and frequencies can be coupled to different energy levels of the artificial atom. (c)-(d) Joint spectral density of two-photon state. (c) Input state of separable two-photon state with Gaussian shape $g(p_1, p_2) = \frac{1}{2\pi\sigma^2} \exp[-(p_1^2 + p_2^2)/2\sigma^2]$, with $p_{1,2}$ is the frequency of the photon and σ is the width of the momentum distribution. (d) Output state. In the calculation, the nonlinear coupling strength $g_d = 3$, the decay rates of the second-harmonic mode $\kappa_{c,0} = \kappa_{c,1} = 1$ and the fundamental mode $\kappa_{a,0} = 1$, $\kappa_{a,1} = 3$, where $\kappa_{a(c),0}$ is the intrinsic decay rate and $\kappa_{a(c),1}$ is the external coupling rate to the waveguide. The spectral width of the input pulse $\sigma = 0.5$. The output two-photon state shows strong spectral correlation.

photonic molecule can be experimentally realized in LN integrated microrings and has been demonstrated to store coherent lasers [32]. The Hamiltonian of the system reads

$$H = H_{AA} + \omega_d d^\dagger d + \sum_{A \in \{a,b\}} (\Omega_A(t) A d^\dagger + h.c.), \quad (2)$$

where d is the bosonic operator for the ancillary mode (frequency ω_d) in the antenna cavity, $A \in \{a,b\}$ is the operator for the modes in the artificial atom. By carefully designing the geometry and tuning of the microresonators, the two cavities have slightly different free spectral ranges. The mode d is detuned from both mode a and b , and the coupling $\Omega_{a,b}(t)$ between d and a or b could be switched by controlling the EO driving. For a strongly over-coupled antenna cavity with external coupling rate $\kappa_{d,1} \gg \kappa_{d,0}$ ($\kappa_{d,0}$ is the intrinsic loss rate of the antenna cavity), it can be adiabatically eliminated and mediates the effective coupling between the waveguide and artificial atom. Considering the input field $A_{in}(t)$ for $A \in \{a,b\}$,

the dynamics of the mode A of artificial atom follows [50]

$$\frac{d}{dt}A = -i[A, H_{AA}] - (\tilde{\kappa}_{A,0} + \tilde{\kappa}_{A,1})A + \sqrt{2\tilde{\kappa}_{A,1}}A_{\text{in}}(t), \quad (3)$$

with $\tilde{\kappa}_{A,0} \approx \kappa_{A,0} + |\Omega_A(t)|^2 \kappa_{d,0}/(\kappa_{d,0} + \kappa_{d,1})^2$ and $\tilde{\kappa}_{A,1} \approx |\Omega_A(t)|^2 \kappa_{d,1}/(\kappa_{d,0} + \kappa_{d,1})^2$ denoting the time-dependent effective external coupling rate controlled by the antenna. By optimizing the shape and frequency of the EO field $\Omega_A(t)$, the antenna can couple photons of different shapes and frequencies in the waveguide to different energy levels. Here, we perform the CZ between identical photons as an instance. To avoid crosstalk during the operation, the non-degenerate $\chi^{(2)}$ interaction is used and the EO drives have different frequencies for two photons to couple them with different energy levels.

Figure 3(b) shows the sequence of the CZ-gate scheme: Initially, quantum states are encoded in control ($|\psi_c\rangle = \alpha_c|0\rangle + \beta_c|1\rangle$) and target ($|\psi_t\rangle = \alpha_t|0\rangle + \beta_t|1\rangle$) photons, which are temporally separated and send to the photonic molecule. These two photons can only be coupled to the artificial atom if they are prepared in state $|1\rangle$. Under appropriate EO drive, the control photon of shape $a_{\text{in}}^c(t)$ is stored into the artificial atom ($|\psi_{AA}\rangle = \alpha_c|000\rangle + \beta_c|100\rangle$). Subsequently, the target photon of shape $b_{\text{in}}^t(t)$ comes and another strong EO drive is applied. Due to the strong $\chi^{(2)}$ interaction, the transition $|100\rangle \rightarrow |110\rangle$ is blocked while $|000\rangle \rightarrow |010\rangle$ is allowed. Thus, the target photon will be reflected back to the waveguide and acquires a π phase depending on the state of the artificial atom. The state becomes $\alpha_c|000\rangle \otimes |\psi_t\rangle + \beta_c|100\rangle \otimes Z|\psi_t\rangle$, manifesting the CZ-gate with Z denotes the Pauli matrix. Finally, another EO drive is applied to retrieve the control photon back to the waveguide. During the whole process, the two photons never meet each other and the two-photon spontaneous emission is avoided.

For a given input Gaussian pulse shape $A_{\text{in}}(t)$ of input photons, the maximum storage and retrieval efficiency

$$\eta_s = \frac{\kappa_{d,1}}{\kappa_{d,0} + \kappa_{d,1}} \quad (4)$$

could be achieved by a carefully tailored driving pulse shape. For retrieval, the optimal drive is derived as

$$\Omega(t) = -i\sqrt{\frac{\kappa_d}{2}} \frac{A_{\text{in}}(t)}{\sqrt{\int_t^\infty dt' |A_{\text{in}}(t')|^2}} \quad (5)$$

(see the SM for details). The optimal drive for the storage process is the time-reverse of that for the retrieval process. It is shown that the quantum storage and retrieval efficiencies are independent of the pulse shape [51], and efficiency higher than 99.9% is expected for the strongly over-coupled antenna due to the very large coupling rate $\kappa_{d,1}/\kappa_{d,0} > 10^3$ between the waveguide and cavity.

For the operations on both the control and target photons, there are at most two excitations, thus the quantum dynamics

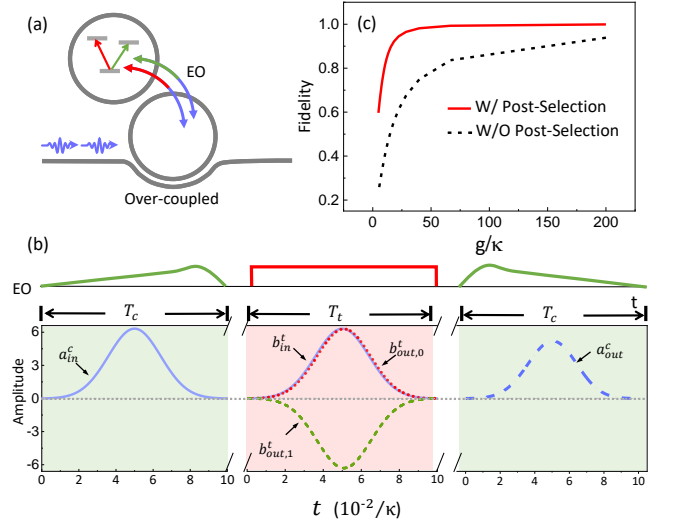


FIG. 3. The photon-photon control-phase gate in a photonic molecule. (a) Schematic of photonic molecule. The cavity coupled to the waveguide serves as an active antenna shown in Fig. 2(b). (b) Time sequence of the EO drive for the quantum storage and retrieval of the photons. At first, the control photon is stored into the artificial atom by time-dependent driving $\Omega_a(t)$. Then the target photon is driven by another EO field with strength $\kappa_{a,0} \ll \Omega_a \ll g$. The output state of the target photon acquires a π phase (shown by the negativity of $b_{\text{out},1}^t$). After the target photon passed, the control photon is retrieved from the artificial atom. In the calculation, $\kappa_{d,1} = 10^3 \kappa_{d,0}$, $\kappa_{d,0} = 2\kappa$, the intrinsic decay rate of the artificial atom $\kappa_{a,0} = \kappa_{b,0} = \kappa = 1$. The pulse shape of the control photon is a Gaussian function $a_{\text{in}}^c = \alpha(\exp(-25(t/T_c - 0.5) - \exp(-6.25)))$, and similar for the target photon b_{in}^t . α is the normalization factor. The duration of the two photons are $T_c = T_t = 0.1/\kappa$. (c) The gate fidelity versus the nonlinear coupling strength g . In our scheme, the pulse shape is maintained with high fidelity. The reason that degrades the gate fidelity is mainly the dissipation of the atomic state, which decays during the transmission of the target photon. By post-selecting the two-photon events, the gate fidelity can be above 99% for $g > 100$.

of the system [Eq. (3)] can be solved in a truncated Fock state space. In Fig. 3(b), we calculated the evolution of the pulse shape for both the control and target photon. It is shown that the shapes of the output fields $b_{\text{out},0}^t$, $b_{\text{out},1}^t$ (subscript 0, 1 denotes the output conditioned on control state $|0\rangle, |1\rangle$) for the target photon and a_{out}^t for the control photon are nearly the same with the input pulses, indicating the high fidelity of the quantum gate. The π phase shift is indicated by the negativity of $b_{\text{out},1}^t$. The relationship between the gate fidelity and g/κ ratio (the atom decay rate $\kappa_{A,0} = \kappa$) is plotted in Fig. 3(c) (dashed line). In our case, the main imperfection affecting the gate fidelity is the lifetime of the atomic states, corresponding to the cavity decay rate κ . By normalizing the output state via post-selection, the gate fidelity can be as high as 99% for $g/\kappa \sim 100$ [Fig. 3(c), solid line].

Recalling that the internal states of an artificial atom could be manipulated through coherent driving [Fig. 1(c)], the artificial atom can also be used for mediating the entanglement be-

tween photons. For example, the Duan-Kimble protocol [52] and the Lindner-Rudolph protocol [53] could be realized without photon storage and retrieval, but requiring the manipulation of the internal state of the artificial atom. These protocols are feasible in light of the fact that two-photon spontaneous emission is avoided. Additionally, the higher excitation eigenstates of the artificial atom can also be engineered to construct quantum gates for the multi-level encoding of quantum states.

Discussion.- From the above studies, the performances of artificial atoms depend on the g/κ , as a benchmark for the cooperation of nonlinear optical processes at the single-photon-level. Among various available photonic platforms, the LN is appealing. It has a significant $\chi^{(2)}$ susceptibility of 3×10^{-11} m/V and excellent electro-optic property. Recent advances on its etching have promoted the quality factor of integrated LN microcavity with a diameter of tens of micrometers up to 10^7 [31]. Therefore, a coupling strength of ~ 5 MHz and a cavity decay rate of ~ 20 MHz are feasible [30], which gives g/κ be about 0.25 and promises to observe the quantum mechanical effect. More excitingly, crystalline LN offers ultralow loss in the telecommunication band and the ultimate quality factor of LN microcavity is higher than 10^9 [32]. By engineering the photonic mode volume and overlap, the value of g/κ could reach 100. Furthermore, the excellent EO property of LN enables dynamical and flexible control of the artificial atoms and photonic structures.

There are also many other potential candidates for artificial atoms. For example, ultra-high-efficiency SHG has been achieved in GaAs microresonators. New materials with excellent nonlinear optics properties, such as organic single crystals [54] and two-dimensional materials [55], are recently developed and are potentially compatible with current PIC platforms [56]. At the same time, new techniques to engineer the $\chi^{(2)}$ nonlinearity have been developed. For example, effective $\chi^{(2)}$ effect could be induced in centrosymmetric materials, such as silicon waveguides by applying external bias electric field [57]. Additionally, a scheme to synthesize and amplify the nonlinear coupling strength with cascaded nonlinear optical processes was proposed recently, and an effective $\chi^{(2)}$ interaction with $g/\kappa > 1$ was predicted with optimal parameters of LN microcavity [58].

Conclusion.- We introduce an artificial atom on the photonic integrated circuit by harnessing the cavity-enhanced optical $\chi^{(2)}$ nonlinearity in a microresonator. Such artificial atom preserves the advantages of both atom and photonic cavity, and offers single-photon level nonlinearity for deterministic quantum gates as well as experimental compatibility and flexibility for scalable quantum devices on a chip. Moreover, we propose a scheme based on the artificial atom to realize high-fidelity two-photon-qubit quantum control-phase gate by switching the coupling channels between the artificial atom and continuum, which also addresses the concerns raised by Shapiro [35, 37]. Due to recent advances in the development of low-loss thin-film LN on insulator platform, the artificial atom with $g/\kappa \sim 1$ is currently feasible, and thereby quantum effects (such as photon blockade) could

be envisioned in a photonic chip maded with pure dielectrics. The universal quantum gate set for quantum information processing would also be achievable with further development of the fabrication and materials. Our work opens an avenue to investigate the quantum nonlinear photonics and is conducive to room-temperature, single-emitter-free quantum information processing.

Note: When finalizing this manuscript, there is a related theoretical work posted on arXiv [59].

Acknowledgments

This work was funded by the National Key R & D Program (Grants No. 2016YFA0301300) and the National Natural Science Foundation of China (Grant No.11874342, 11934012, 11922411, 11904316, and 11704370), and Anhui Initiative in Quantum Information Technologies (AHY130200).

* chunhua@ustc.edu.cn

† clzou321@ustc.edu.cn

- [1] A. Politi, J. C. F. Matthews, M. G. Thompson, and J. L. O'Brien, Integrated quantum photonics, *IEEE Journal of Selected Topics in Quantum Electronics* **15**, 1673 (2009).
- [2] S. Takeda and A. Furusawa, Toward large-scale fault-tolerant universal photonic quantum computing, *APL Photonics* **4**, 060902 (2019).
- [3] T. D. Ladd, F. Jelezko, R. Laflamme, Y. Nakamura, C. Monroe, and J. L. O'Brien, Quantum computers, *Nature* **464**, 45 (2010).
- [4] A. Aspuru-Guzik and P. Walther, Photonic quantum simulators, *Nature Physics* **8**, 285 (2012).
- [5] A. Politi, J. C. F. Matthews, and J. L. O'Brien, Shor's quantum factoring algorithm on a photonic chip, *Science* **325**, 1221 (2009).
- [6] L. Caspani, C. Xiong, B. J. Eggleton, D. Bajoni, M. Liscidini, M. Galli, R. Morandotti, and D. J. Moss, Integrated sources of photon quantum states based on nonlinear optics, *Light: Science & Applications* **6**, e17100 (2017).
- [7] A. Politi, M. J. Cryan, J. G. Rarity, S. Yu, and J. L. O'Brien, Silica-on-silicon waveguide quantum circuits, *Science* **320**, 646 (2008).
- [8] A. Crespi, R. Ramponi, R. Osellame, L. Sansoni, I. Bongioanni, F. Sciarrino, G. Vallone, and P. Mataloni, Integrated photonic quantum gates for polarization qubits, *Nature Communications* **2**, 566 (2011).
- [9] F. Najafi, J. Mower, N. C. Harris, F. Bellei, A. Dane, C. Lee, X. Hu, P. Kharel, F. Marsili, S. Assefa, K. K. Berggren, and D. Englund, On-chip detection of non-classical light by scalable integration of single-photon detectors, *Nature Communications* **6**, 5873 (2015).
- [10] R. Cheng, X. Guo, X. Ma, L. Fan, K. Y. Fong, M. Poot, and H. X. Tang, Self-aligned multi-channel superconducting nanowire single-photon detectors, *Opt. Express* **24**, 27070 (2016).
- [11] J. P. Sprengers, A. Gaggero, D. Sahin, S. Jahanmirinejad, G. Frucci, F. Mattioli, R. Leoni, J. Beetz, M. Lerner, M. Kamp, S. Höfling, R. Sanjines, and A. Fiore, Waveguide superconducting single-photon detectors for integrated quantum photonic circuits, *Appl. Phys. Lett.* **99**, 181110 (2019).
- [12] S. Khasminskaya, F. Pyatkov, K. Słowik, S. Ferrari, O. Kahl, V. Kovalyuk, P. Rath, A. Vetter, F. Hennrich, M. M. Kappes,

- G. Gol'tsman, A. Korneev, C. Rockstuhl, R. Krupke, and W. H. P. Pernice, Fully integrated quantum photonic circuit with an electrically driven light source, *Nature Photonics* **10**, 727 (2016).
- [13] R. W. Boyd, *Nonlinear optics* (Academic press 2003).
- [14] M. A. Nielsen and I. L. Chuang, *Quantum Computation and Quantum Information* (Cambridge University Press, Cambridge 2010).
- [15] J. L. O'Brien, A. Furusawa, and J. Vučković, Photonic quantum technologies, *Nature Photonics* **3**, 687 (2009).
- [16] A. V. Gorshkov, J. Otterbach, M. Fleischhauer, T. Pohl, and M. D. Lukin, Photon-photon interactions via rydberg blockade, *Phys. Rev. Lett.* **107**, 133602 (2011).
- [17] T. G. Tiecke, J. D. Thompson, N. P. de Leon, L. R. Liu, V. Vuletić, and M. D. Lukin, Nanophotonic quantum phase switch with a single atom, *Nature* **508**, 241 (2014).
- [18] B. Hacker, S. Welte, G. Rempe, and S. Ritter, A photon-photon quantum gate based on a single atom in an optical resonator, *Nature* **536**, 193 (2016).
- [19] K. J. Vahala, Optical microcavities, *Nature* **424**, 839 (2003).
- [20] D. V. Strekalov, C. Marquardt, A. B. Matsko, H. G. Schwefel, and G. Leuchs, Nonlinear and quantum optics with whispering gallery resonators, *J. Opt.* **18**, 123002 (2016).
- [21] G. Lin, A. Coillet, and Y. K. Chembo, Nonlinear photonics with high-q whispering-gallery-mode resonators, *Adv. Opt. Photon.* **9**, 828 (2017).
- [22] A. W. Bruch, X. Liu, J. B. Surya, C.-L. Zou, and H. X. Tang, On-chip $\chi^{(2)}$ microring optical parametric oscillator, arXiv:1909.07422 (2019).
- [23] Q. Li, M. Davanço, and K. Srinivasan, Efficient and low-noise single-photon-level frequency conversion interfaces using silicon nanophotonics, *Nature Photonics* **10**, 406 (2016).
- [24] X. Guo, C. L. Zou, H. Jung, and H. X. Tang, On-Chip Strong Coupling and Efficient Frequency Conversion between Telecom and Visible Optical Modes, *Phys. Rev. Lett.* **117**, 1 (2016), 1511.08112.
- [25] T. J. Kippenberg, A. L. Gaeta, M. Lipson, and M. L. Gorodetsky, Dissipative kerr solitons in optical microresonators, *Science* **361**, eaan8083 (2018).
- [26] M. Li, C.-L. Zou, C.-H. Dong, and D.-X. Dai, Optimal third-harmonic generation in an optical microcavity with $\chi^{(2)}$ and $\chi^{(3)}$ nonlinearities, *Optics express* **26**, 27294 (2018).
- [27] A. W. Bruch, X. Liu, X. Guo, J. B. Surya, Z. Gong, L. Zhang, J. Wang, J. Yan, and H. X. Tang, 17000 %/w second-harmonic conversion efficiency in single-crystalline aluminum nitride microresonators, *Appl. Phys. Lett.* **113**, 131102 (2019).
- [28] L. Chang, A. Boes, P. Pintus, J. D. Peters, M. Kennedy, X.-W. Guo, N. Volet, S.-P. Yu, S. B. Papp, and J. E. Bowers, Strong frequency conversion in heterogeneously integrated gas resonators, *APL Photonics* **4**, 036103 (2019).
- [29] J. Lin, N. Yao, Z. Hao, J. Zhang, W. Mao, M. Wang, W. Chu, R. Wu, Z. Fang, L. Qiao, W. Fang, F. Bo, and Y. Cheng, Broadband quasi-phase-matched harmonic generation in an on-chip monocrystalline lithium niobate microdisk resonator, *Phys. Rev. Lett.* **122**, 173903 (2019).
- [30] J. Lu, J. B. Surya, X. Liu, A. W. Bruch, Z. Gong, Y. Xu, and H. X. Tang, Periodically poled thin film lithium niobate microring resonators with a second-harmonic generation efficiency of 250,000 %/W, Unpublished (2019).
- [31] M. Zhang, C. Wang, R. Cheng, A. Shams-Ansari, and M. Lončar, Monolithic ultra-high-q lithium niobate microring resonator, *Optica* **4**, 1536 (2017).
- [32] M. Zhang, C. Wang, Y. Hu, A. Shams-Ansari, T. Ren, S. Fan, and M. Lončar, Electronically programmable photonic molecule, *Nature Photonics* **13**, 36 (2019).
- [33] J.-Y. Chen, Z.-H. Ma, Y. M. Sua, Z. Li, C. Tang, and Y.-P. Huang, Ultra-efficient frequency conversion in quasi-phase-matched lithium niobate microrings, *Optica* **6**, 1244 (2019).
- [34] X. Guo, C. Zou, and H. Tang, Second-harmonic generation in aluminum nitride microrings with 2500 %/W conversion efficiency, *Optica* **3**, 1126 (2016).
- [35] J. H. Shapiro, Single-photon kerr nonlinearities do not help quantum computation, *Phys. Rev. A* **73**, 062305 (2006).
- [36] J. Gea-Banacloche, Impossibility of large phase shifts via the giant kerr effect with single-photon wave packets, *Phys. Rev. A* **81**, 043823 (2010).
- [37] J. Dove, C. Chudzicki, and J. H. Shapiro, Phase-noise limitations on single-photon cross-phase modulation with differing group velocities, *Phys. Rev. A* **90**, 062314 (2014).
- [38] C. Chudzicki, I. L. Chuang, and J. H. Shapiro, Deterministic and cascaded conditional phase gate for photonic qubits, *Phys. Rev. A* **87**, 042325 (2013).
- [39] D. J. Brod and J. Combes, Passive cphase gate via cross-kerr nonlinearities, *Phys. Rev. Lett.* **117**, 080502 (2016).
- [40] K. Xia, M. Johnsson, P. L. Knight, and J. Twamley, Cavity-free scheme for nondestructive detection of a single optical photon, *Phys. Rev. Lett.* **116**, 023601 (2016).
- [41] S. Ferretti and D. Gerace, Single-photon nonlinear optics with kerr-type nanostructured materials, *Phys. Rev. B* **85**, 033303 (2012).
- [42] A. Majumdar and D. Gerace, Single-photon blockade in doubly resonant nanocavities with second-order nonlinearity, *Phys. Rev. B* **87**, 235319 (2013).
- [43] C. Hamsen, K. N. Tolazzi, T. Wilk, and G. Rempe, Two-photon blockade in an atom-driven cavity qed system, *Phys. Rev. Lett.* **118**, 133604 (2017).
- [44] P. Krantz, M. Kjaergaard, F. Yan, T. P. Orlando, S. Gustavsson, and W. D. Oliver, A quantum engineer's guide to superconducting qubits, *Applied Physics Reviews* **6**, 021318 (2019).
- [45] P. Lodahl, S. Mahmoodian, S. Stobbe, A. Rauschenbeutel, P. Schneeweiss, J. Volz, H. Pichler, and P. Zoller, Chiral quantum optics, *Nature* **541**, 473 (2017).
- [46] H. Zheng, D. J. Gauthier, and H. U. Baranger, Waveguide-QED-Based Photonic Quantum Computation, *Physical Review Letters* **111**, 090502 (2013).
- [47] J.-T. Shen and S. Fan, Strongly correlated two-photon transport in a one-dimensional waveguide coupled to a two-level system, *Phys. Rev. Lett.* **98**, 153003 (2007).
- [48] C. Lee, C. Noh, N. Schetakis, and D. G. Angelakis, Few-photon transport in many-body photonic systems: A scattering approach, *Phys. Rev. A* **92**, 063817 (2015).
- [49] S. Xu and S. Fan, Input-output formalism for few-photon transport: A systematic treatment beyond two photons, *Phys. Rev. A* **91**, 043845 (2015).
- [50] D. F. Walls and G. J. Milburn, *Quantum optics* (Springer Science & Business Media 2007).
- [51] A. V. Gorshkov, A. André, M. D. Lukin, and A. S. Sørensen, Photon storage in Λ -type optically dense atomic media. i. cavity model, *Phys. Rev. A* **76**, 033804 (2007).
- [52] L.-M. Duan and H. J. Kimble, Scalable photonic quantum computation through cavity-assisted interactions, *Phys. Rev. Lett.* **92**, 127902 (2004).
- [53] N. H. Lindner and T. Rudolph, Proposal for Pulsed On-Demand Sources of Photonic Cluster State Strings, *Physical Review Letters* **103**, 113602 (2009).
- [54] M. Jazbinsek, L. Mutter, and P. Gunter, Photonic applications with the organic nonlinear optical crystal dast, *IEEE Journal of*

Selected Topics in Quantum Electronics **14**, 1298 (Sept).

- [55] A. Majumdar, C. M. Dodson, T. K. Fryett, A. Zhan, S. Buckley, and D. Gerace, Hybrid 2d material nanophotonics: A scalable platform for low-power nonlinear and quantum optics, *ACS Photonics* **2**, 1160 (2015).
- [56] M. Li, L. Zhang, L.-M. Tong, and D.-X. Dai, Hybrid silicon nonlinear photonics [invited], *Photon. Res.* **6**, B13 (2018).
- [57] E. Timurdogan, C. V. Poulton, M. J. Byrd, and M. R. Watts, Electric field-induced second-order nonlinear optical effects in silicon waveguides, *Nature Photonics* **11**, 200 (2017).
- [58] M. Li and C.-L. Zou, Nonlinearity amplification with synthetic nonlinearity, Unpublished (2019).
- [59] M. Heuck, K. Jacobs, and D. R. Englund, Controlled-phase Gate using Dynamically Coupled Cavities and Optical Nonlinearities, arXiv:1909.05751 (2019).
- [60] J.-T. Shen and S. Fan, Strongly correlated multiparticle transport in one dimension through a quantum impurity, *Phys. Rev. A* **76**, 062709 (2007).

SUPPLEMENTARY MATERIAL

I. ANHARMONIC ENERGY LEVEL STRUCTURE OF ARTIFICIAL ATOMS

The cavity, which is designed for phase-matching condition that enables non-degenerate $\chi^{(2)}$ interaction $\omega_a + \omega_b \rightarrow \omega_c$, has a Hamiltonian of

$$H = \omega_a a^\dagger a + \omega_b b^\dagger b + \omega_c c^\dagger c + g_{\text{nd}} (a^\dagger b^\dagger c + abc^\dagger), \quad (\text{S.1})$$

where a, b, c represents the bosonic operator for modes, g_{nd} is the nonlinear coupling strength. In the strong coupling regime $g_{\text{nd}} \gtrsim \kappa_a, \kappa_b, \kappa_c$, the system shows strong anharmonicity. For example, the state $|1_a 1_b 0_c\rangle$ will couple to $|0_a 0_b 1_c\rangle$ with a strength of g_{nd} , and these two states will be hybridized with each other, leading to a splitting of $2g_{\text{nd}}$. In this nonlinear cavity system, the eigenstates and eigenvalues in each N -photon subspace could be solved independently. The energy conversation requires

$$N = N_a + N_b + 2N_c, \quad (\text{S.2})$$

where N_i is the number of excitation in mode i ($i \in \{a, b, c\}$). Therefore, the basis $\{|\Psi_{N,m,n}\rangle = |m-1, n-1, N-m-n+2\rangle\}_N$ spans the N -photon subspace $H^{(N)}$, where $m, n \leq N$ are integers with $m+n-2 < N$. The Hamiltonian is written in the matrix form as

$$H^{(N)} = \sum H_{m,n;m',n'}^{(N)} |\Psi_{N,m,n}\rangle \langle \Psi_{N,m',n'}|, \quad (\text{S.3})$$

with the matrix element

$$H_{m,n;m',n'}^{(N)} = \langle \Psi_{N,m',n'} | H | \Psi_{N,m,n} \rangle. \quad (\text{S.4})$$

The eigenstates and eigenenergies are solved by diagonalizing the matrix. Specially, we only consider the interaction between two photons, thus truncate the dimension of the Fock state space to 2 is enough. The Hamiltonian in 2-photon excitation is spanned by the eigenstate $|\tilde{j}\rangle \in \{|1, 1, 0\rangle, |0, 0, 1\rangle\}$. For perfect phase matching, an appropriate rotating frame can be chosen to transform H to $H = g(a^\dagger b^\dagger c + abc^\dagger)$,

$$H_{ij}^2 = \langle \tilde{j} | H | \tilde{i} \rangle_2 \quad (\text{S.5})$$

$$= g_{\text{nd}} (\delta(i-1, j) + \delta(i, j-1)), \quad (\text{S.6})$$

where $\delta(x, y)$ is the Kronecker delta function. The energy levels are obtained by diagonalizing the matrix of the Hamiltonian. Therefore, the degeneracy of the two-excitation states is removed by the nonlinear interaction with energy levels split by $2g_{\text{nd}}$. If the cavity is initially prepared in the state $|1_a 0_b 0_c\rangle$, the photon resonant with mode b can no longer efficiently induce the transition from $|1_a 0_b 0_c\rangle$ to $|0_a 0_b 1_c\rangle$, which is known as the photon-blockade effect. The energy levels of second-harmonic generation $g_d(a^{\dagger 2}c + a^2c^\dagger)$ can be obtained following a similar calculation.

II. TWO-PHOTON SCATTERING BY THE ARTIFICIAL ATOM

In this section, we investigate the two-photon transport through a waveguide side-coupled to a cavity supporting $\chi^{(2)}$ interaction. Figure 2(a) in the main text schematically illustrates a doubly-resonant microcavity coupled with a bus waveguide. The two resonant modes in the cavity are the fundamental (FM) mode a and the second-harmonic (SH) mode c with frequency ω_i ($i \in \{a, c\}$). The waveguide supports continuum states both in the fundamental and SH frequency bands. Inside the cavity, modes a and c couple with each other via the process of SH generation. The Hamiltonian of whole system includes, the continuum states in the waveguide

$$H_W = \int dx f^\dagger(x) \frac{1}{i} \frac{d}{dx} f(x) + \int dx s^\dagger(x) \frac{1}{i} \frac{d}{dx} s(x), \quad (\text{S.7})$$

the localized states in the cavity

$$H_C = (\omega_a - i\kappa_{a,0}) a^\dagger a + (\omega_c - i\kappa_{c,0}) c^\dagger c, \quad (\text{S.8})$$

the nonlinear coupling inside the cavity

$$H_{nl} = g_d (a^{\dagger 2} c + a^2 c^\dagger), \quad (\text{S.9})$$

the linear coupling between the waveguide and cavity

$$H_l = V_a \int dx \delta(x) [f^\dagger(x)a + f(x)a^\dagger] + V_c \int dx \delta(x) [s^\dagger(x)c + s(x)c^\dagger], \quad (\text{S.10})$$

where x is coordinate along the waveguide, $f(x)$ ($s(x)$) and $f^\dagger(x)$ ($s^\dagger(x)$) are the annihilation and creation operators at position x in the waveguide, g_d is the nonlinear coupling strength of SH generation, V_a (V_c) is the coupling strength between waveguide and cavity in the fundamental (SH) frequency band, $\kappa_{a,0}$ ($\kappa_{c,0}$) is the intrinsic decay rates of the cavity mode. Since the coupling near the narrow resonant frequency window is considered, the dispersions of the coupling strengths g_d , V_a and V_c are neglected. The input state is initially prepared in a two-photon state at the fundamental frequencies. A general form of two-excitation state can be written as

$$|E_2\rangle = \int dx_1 dx_2 g(x_1, x_2) f^\dagger(x_1) f^\dagger(x_2) |0\rangle + \int dx m(x) f^\dagger(x) |0\rangle + \int dx h(x) s^\dagger(x) |0\rangle + f_a \frac{1}{\sqrt{2}} a^\dagger a^\dagger |0\rangle + f_c c^\dagger |0\rangle. \quad (\text{S.11})$$

Following the Schrodinger equation $H|E_2\rangle = E_2|E_2\rangle$ ($E_2 = k_1 + k_2$, k_i is the frequency of the i -th photon), one gets

$$\left(-i\frac{\partial}{\partial x_1} - i\frac{\partial}{\partial x_2} - E_2\right) g(x_1, x_2) + \frac{V_a}{2} [\delta(x_1)m(x_2) + \delta(x_2)m(x_1)] = 0, \quad (\text{S.12})$$

$$\left(-i\frac{d}{dx} + \omega_a - i\kappa_{a,0} - E_2\right) m(x) + V_a [g(x, 0) + g(0, x)] + \sqrt{2}V_a f_a \delta(x) = 0, \quad (\text{S.13})$$

$$\left(-i\frac{d}{dx} - E_2\right) h(x) + V_c f_c \delta(x) = 0, \quad (\text{S.14})$$

$$(2\omega_a - 2i\kappa_{a,0} - E_2) f_a + \sqrt{2}g_d f_c + \sqrt{2}V_a m(0) = 0, \quad (\text{S.15})$$

$$(\omega_c - i\kappa_{c,0} - E_2) f_c + \sqrt{2}g_d f_a + V_c h(0) = 0. \quad (\text{S.16})$$

The discontinuous functions fulfills

$$g(x, 0) = g(0, x), \quad (\text{S.17})$$

$$g(x, 0) = [g(x, 0^+) + g(x, 0^-)]/2, \quad (\text{S.18})$$

$$m(0) = [m(0^+) + m(0^-)]/2, \quad (\text{S.19})$$

$$h(0) = [h(0^+) + h(0^-)]/2, \quad (\text{S.20})$$

$$\frac{d}{dx} m(x)|_{x=0} = [m(0^+) - m(0^-)] \delta(x). \quad (\text{S.21})$$

Then Eqs.(S.12)-(S.16) are equivalent to

$$\left(-i\frac{\partial}{\partial x_1} - i\frac{\partial}{\partial x_2} - E_2\right) g(x_1, x_2) = 0, \quad (\text{S.22})$$

$$\frac{2i}{V_a} [g(0^+, x) - g(0^-, x)] = m(x), \quad (\text{S.23})$$

$$\left(-i\frac{d}{dx} + \omega_a - i\kappa_{a,0} - E_2\right) m(x) + V_a [g(x, 0^+) + g(0^-, x)] = 0, \quad (\text{S.24})$$

$$\frac{i}{\sqrt{2}V_a} [m(0^+) - m(0^-)] = f_a, \quad (\text{S.25})$$

$$\left(-i\frac{d}{dx} - E_2\right) h(x) = 0, \quad (\text{S.26})$$

$$\frac{i}{V_c} [h(0^+) - h(0^-)] = f_c, \quad (\text{S.27})$$

$$(2\omega_a - 2i\kappa_{a,0} - E_2) f_a + \sqrt{2}g_d f_c + \sqrt{2}V_a m(0) = 0, \quad (\text{S.28})$$

$$(\omega_c - i\kappa_{c,0} - E_2) f_c + \sqrt{2}g_d f_a + V_c h(0) = 0. \quad (\text{S.29})$$

Combine Eqs. (S.23) and (S.24), we get

$$\left(-i\frac{d}{dx} + \omega_a - i\kappa_{a,0} - i\kappa_{a,1} - E_2\right) g(0^+, x) = \left(-i\frac{d}{dx} + \omega_a - i\kappa_{a,0} + i\kappa_{a,1} - E_2\right) g(0^-, x). \quad (\text{S.30})$$

Adopting the method in Ref. [46], $g(x_1, x_2)$ is divided to three regions: $g_1(x_1, x_2)$ for $x_1 \leq x_2 < 0$, $g_2(x_1, x_2)$ for $x_1 < 0 < x_2$ and $g_3(x_1, x_2)$ for $0 < x_1 \leq x_2$. For two-photon monochromatic wave input state

$$g_1(x_1, x_2) = \frac{1}{2\sqrt{2}\pi} \left(e^{ik_1x_1} e^{ik_2x_2} + e^{ik_2x_1} e^{ik_1x_2} \right), \quad (\text{S.31})$$

$g(x_1, x_2)$ in the other two regions are derived from Eq. (S.30) as

$$g_2(x_1, x_2) = \frac{1}{2\sqrt{2}\pi} \left(t_{k_2} e^{i(k_1x_1+k_2x_2)} + t_{k_1} e^{i(k_2x_1+k_1x_2)} \right), \quad (\text{S.32})$$

$$g_3(x_1, x_2) = \frac{1}{2\sqrt{2}\pi} t_{k_1} t_{k_2} \left(e^{i(k_1x_1+k_2x_2)} + e^{i(k_2x_1+k_1x_2)} \right) + B e^{-i(\omega_a - i\kappa_{a,0} - i\kappa_{a,1})(x_2 - x_1)} e^{i(k_1+k_2)x_2}, \quad (\text{S.33})$$

with

$$t_k = \frac{k - \omega_a + i\kappa_{a,0} - i\kappa_{a,1}}{k - \omega_a + i\kappa_{a,0} + i\kappa_{a,1}}. \quad (\text{S.34})$$

Eliminating f_a and f_c ,

$$\frac{2i}{V_a} [\alpha_a^- g(0^+, 0^+) - (\alpha_a^- + \alpha_a^+) g(0^-, 0^+) + \alpha_a^+ g(0^-, 0^-)] + 2g_d \frac{V_a}{V_c} [h(0^+) - h(0^-)] = 0, \quad (\text{S.35})$$

$$\alpha_b^- h(0^+) - \alpha_b^+ h(0^-) + \frac{2ig_d V_c}{V_a^2} [g(0^+, 0^+) - 2g(0^-, 0^+) + g(0^-, 0^-)] = 0, \quad (\text{S.36})$$

with $\alpha_a^\pm = 2(\omega_a - i\kappa_{a,0} \pm i\kappa_{a,1}) - k_1 - k_2$, $\alpha_c^\pm = (\omega_c - i\kappa_{c,0} \pm i\kappa_{c,1}) - k_1 - k_2$, $\kappa_{i,1} = V_i^2/2$. Using the values at the discontinuous points,

$$g(0^+, 0^+) = g_3(0, 0) = \frac{1}{\sqrt{2}\pi} t_{k_1} t_{k_2} + B, \quad (\text{S.37})$$

$$g(0^-, 0^+) = g_2(0, 0) = \frac{1}{2\sqrt{2}\pi} (t_{k_1} + t_{k_2}), \quad (\text{S.38})$$

$$g(0^-, 0^-) = g_1(0, 0) = \frac{1}{\sqrt{2}\pi}, \quad (\text{S.39})$$

$$h(0^+) = \frac{1}{\sqrt{2}\pi} C, \quad (\text{S.40})$$

$$h(0^-) = 0, \quad (\text{S.41})$$

one finally obtains

$$\begin{aligned} C &= \frac{ig_d \sqrt{2\kappa_{c,1}} (\alpha_a^+ - \alpha_a^-) (2 - t_{k_1} - t_{k_2})}{2\sqrt{\pi} \kappa_{a,1} (\alpha_a^- \alpha_c^- - 2g_d^2)} \\ &= -\frac{2g_d \sqrt{2\kappa_{c,1}} (2 - t_{k_1} - t_{k_2})}{\sqrt{\pi} (\alpha_a^- \alpha_c^- - 2g_d^2)}, \end{aligned} \quad (\text{S.42})$$

$$\begin{aligned} B &= \frac{4g_d^2 (t_{k_1} - 1) (t_{k_2} - 1) + \alpha_a^+ \alpha_c^- (t_{k_1} + t_{k_2} - 2) + \alpha_a^- \alpha_c^- (t_{k_1} + t_{k_2} - 2t_{k_1} t_{k_2})}{2\sqrt{2}\pi (\alpha_a^- \alpha_c^- - 2g_d^2)} \\ &= \frac{\sqrt{2}g_d^2 (1 - t_{k_1}) (1 - t_{k_2})}{\pi (\alpha_a^- \alpha_c^- - 2g_d^2)}. \end{aligned} \quad (\text{S.43})$$

The expressions can be simplified as

$$C = -\frac{2g_d \sqrt{2\kappa_{c,1}}}{\sqrt{\pi} [2\omega_a - k_1 - k_2 - 2i\kappa_{a,tot}] [\omega_c - k_1 - k_2 - i\kappa_{c,tot}] - 2g_d^2} \left(\frac{2i\kappa_{a,1}}{k_1 - \omega_a + i\kappa_{a,tot}} + \frac{2i\kappa_{a,1}}{k_2 - \omega_a + i\kappa_{a,tot}} \right), \quad (\text{S.44})$$

$$B = \frac{\sqrt{2}g_d^2}{\pi [2\omega_a - k_1 - k_2 - 2i\kappa_{a,tot}] [\omega_c - k_1 - k_2 - i\kappa_{c,tot}] - 2g_d^2} \frac{2i\kappa_{a,1}}{k_1 - \omega_a + i\kappa_{a,tot}} \frac{2i\kappa_{a,1}}{k_2 - \omega_a + i\kappa_{a,tot}}. \quad (\text{S.45})$$

where $\kappa_{i,tot} = \kappa_{i,0} + \kappa_{i,1}$. The wave-functions of two-photon input and output states are computed by the Lippmann-Schwinger equations [60],

$$\begin{aligned}\phi_{in}(x_1, x_2) &= \langle x_1, x_2 | E_2 \rangle - \langle x_1, x_2 | \frac{1}{k_1 + k_2 - H_0 + i0^+} H_{int} | E_2 \rangle \\ &= g_1(x_1, x_2) \theta(x_2 - x_1) + g_1(x_2, x_1) \theta(x_1 - x_2),\end{aligned}\quad (S.46)$$

$$\begin{aligned}\phi_{out}(x_1, x_2) &= \langle x_1, x_2 | E_2 \rangle - \langle x_1, x_2 | \frac{1}{k_1 + k_2 - H_0 - i0^+} H_{int} | E_2 \rangle \\ &= g_3(x_1, x_2) \theta(x_2 - x_1) + g_3(x_2, x_1) \theta(x_1 - x_2).\end{aligned}\quad (S.47)$$

Then the two-photon scattering matrix is obtained by calculating the wave-function overlap between the output state and the two photon plain wave state,

$$S(p_1, p_2; k_1, k_2) = \int dx_1 dx_2 \frac{1}{2\sqrt{2}\pi} [e^{-i(p_1 x_1 + p_2 x_2)} + e^{-i(p_2 x_1 + p_1 x_2)}] \phi_{out}(x_1, x_2). \quad (S.48)$$

The transmission plane wave term is

$$\begin{aligned}S_{plane} &= \frac{1}{8\pi^2} \int dx_1 dx_2 [e^{-i(p_1 - k_1)x_1} e^{-i(p_2 - k_2)x_2} + e^{-i(p_1 - k_2)x_1} e^{-i(p_2 - k_1)x_2} \\ &\quad + e^{-i(p_1 - k_2)x_2} e^{-i(p_2 - k_1)x_1} + e^{-i(p_2 - k_2)x_1} e^{-i(p_1 - k_1)x_2}] \\ &= t_{k_1} t_{k_2} [\delta(p_1 - k_1) \delta(p_2 - k_2) + \delta(p_1 - k_2) \delta(p_2 - k_1)] \\ &= S_{p_1 k_1} S_{p_2 k_2} + S_{p_1 k_2} S_{p_2 k_1}.\end{aligned}\quad (S.49)$$

The bound state term is

$$\begin{aligned}S_{bound} &= \frac{B}{2\sqrt{2}\pi} \int dx_1 dx_2 [e^{-i(p_1 x_1 + p_2 x_2)} + e^{-i(p_2 x_1 + p_1 x_2)}] e^{-i(\omega_a - i\kappa_{a,0} - i\kappa_{a,1})(x_2 - x_1)} e^{i(k_1 + k_2)x_2} \theta(x_2 - x_1) + \\ &\quad \frac{B}{2\sqrt{2}\pi} \int dx_1 dx_2 [e^{-i(p_1 x_1 + p_2 x_2)} + e^{-i(p_2 x_1 + p_1 x_2)}] e^{-i(\omega_a - i\kappa_{a,0} - i\kappa_{a,1})(x_1 - x_2)} e^{i(k_1 + k_2)x_1} \theta(x_1 - x_2).\end{aligned}\quad (S.50)$$

The integral of the first term is simplified by replacing x_2 by $x_3 + x_1$ and similar for the second term. We get

$$\begin{aligned}S_{bound,1} &= \frac{B}{2\sqrt{2}\pi} \int dx_1 dx_3 e^{-(\kappa_{a,0} + \kappa_{a,1})x_3} [e^{-i(p_1 + p_2 - k_1 - k_2)x_1} e^{-i(p_2 + \omega_a - k_1 - k_2)x_3} \\ &\quad + e^{-i(p_1 + p_2 - k_1 - k_2)x_1} e^{-i(p_1 + \omega_a - k_1 - k_2)x_3}] \theta(x_3) \\ &= \frac{B}{2\sqrt{2}\pi} \times 2\pi \left[\frac{1}{(\kappa_{a,0} + \kappa_{a,1}) + i(p_2 + \omega_a - k_1 - k_2)} \delta(p_1 + p_2 - k_1 - k_2) \right. \\ &\quad \left. + \frac{1}{(\kappa_{a,0} + \kappa_{a,1}) + i(p_1 + \omega_a - k_1 - k_2)} \delta(p_1 + p_2 - k_1 - k_2) \right] \\ &= \frac{B}{\sqrt{2}} \left[\frac{i}{p_1 - \omega_a + i(\kappa_{a,0} + \kappa_{a,1})} + \frac{i}{p_2 - \omega_a + i(\kappa_{a,0} + \kappa_{a,1})} \right] \delta(p_1 + p_2 - k_1 - k_2).\end{aligned}\quad (S.51)$$

Due to the symmetry of the wavefunction

$$\begin{aligned}S_{bound} &= 2S_{bound,1} \\ &= \sqrt{2}B \left[\frac{i}{p_1 - \omega_a + i(\kappa_{a,0} + \kappa_{a,1})} + \frac{i}{p_2 - \omega_a + i(\kappa_{a,0} + \kappa_{a,1})} \right] \delta(p_1 + p_2 - k_1 - k_2) \\ &= \sqrt{2}B \left[\frac{i}{p_1 - \omega_a + i(\kappa_{a,0} + \kappa_{a,1})} + \frac{i}{p_2 - \omega_a + i(\kappa_{a,0} + \kappa_{a,1})} \right] \delta(p_1 + p_2 - k_1 - k_2) \\ &= \frac{B}{\sqrt{2}\kappa_{a,1}} (2 - t_{p_1} - t_{p_2}) \delta(p_1 + p_2 - k_1 - k_2).\end{aligned}\quad (S.52)$$

The total scattering matrix is

$$S(p_1, p_2; k_1, k_2) = t_{k_1} t_{k_2} [\delta(p_1 - k_1) \delta(p_2 - k_2) + \delta(p_1 - k_2) \delta(p_2 - k_1)] \quad (S.53)$$

$$+ \frac{B}{\sqrt{2}\kappa_{a,1}} (2 - t_{p_1} - t_{p_2}) \delta(p_1 + p_2 - k_1 - k_2). \quad (S.54)$$

According to the scattering matrix, one can compute the output spectrum of the two-photon state as

$$\alpha_{out}(p_1, p_2) = \int \int \alpha_{in}(k_1, k_2) S(p_1, p_2; k_1, k_2) dk_1 dk_2, \quad (\text{S.55})$$

where $\alpha_{in}(k_1, k_2)$ is the input spectrum.

From the frequency conversion point of view, one might care about the conversion efficiency of the two-photon second-harmonic generation. The two-photon to one-photon conversion matrix is

$$\begin{aligned} S(p; k_1, k_2) &= \int dx e^{-ipx} \frac{1}{\sqrt{2\pi}} C(k_1 + k_2) e^{i(k_1 + k_2)x} \\ &= \frac{1}{\sqrt{2\pi}} C(k_1 + k_2) \int dx e^{-i(p - k_1 - k_2)x} \\ &= C(k_1 + k_2) \delta(p - k_1 - k_2). \end{aligned} \quad (\text{S.56})$$

The output spectrum of the second-harmonic photon is

$$\begin{aligned} \beta_{out}(p) &= \int \int \alpha_{in}(k_1, k_2) S(p; k_1, k_2) dk_1 dk_2 \\ &= \int \int \alpha_{in}(k_1, k_2) C(k_1 + k_2) \delta(p - k_1 - k_2) dk_1 dk_2. \end{aligned} \quad (\text{S.57})$$

Then, we get the conversion efficiency

$$\eta = \frac{\int |\beta_{out}(p)|^2 dp}{2 \int \int |\alpha_{in}(k_1, k_2)|^2 dk_1 dk_2}. \quad (\text{S.58})$$

III. CONTROL PHASE GATE VIA PHOTONIC MOLECULE

A. Coupled microresonator

In our scheme, an active antenna is used to couple the traveling photons and the artificial atom, as shown by Fig. 3 in the main text. For artificial atom supporting mode a, b (with resonant frequency ω_a, ω_b), drive field with frequency $\omega_{EO} = \omega_A - \omega_0$ can be used to induce the coupling between photons of frequency ω_0 and the mode A ($A \in \{a, b\}$). Such an antenna can be physically realized with a microcavity and electro-optic (EO) effect [32]. A microwave driving is applied on the two cavities which shifts the two cavity resonant frequencies to opposite directions, with the photonic molecular Hamiltonian as

$$H = \omega_{m,1} m_1^\dagger m_1 + \omega_{m,2} m_2^\dagger m_2 + J (m_1^\dagger m_2 + m_1 m_2^\dagger) + G \cos(\omega_{EO} t) (m_1^\dagger m_1 - m_2^\dagger m_2), \quad (\text{S.59})$$

where $\omega_{m,i}$ is the resonant frequency of the cavity mode m_i , J is the linear coupling strength between the two cavities, G is the coupling strength due to $\chi^{(2)}$ interaction between photonic mode and electric field, i.e. the EO drive. Denoting $\omega_0 = \frac{\omega_{m,1} + \omega_{m,2}}{2}$, $\delta\omega = \frac{\omega_{m,1} - \omega_{m,2}}{2}$, $\tan \theta = \frac{J}{\delta\omega}$ and making the linear transformation

$$b = \cos \frac{\theta}{2} m_1 + \sin \frac{\theta}{2} m_2, \quad (\text{S.60})$$

$$d = -\sin \frac{\theta}{2} m_1 + \cos \frac{\theta}{2} m_2, \quad (\text{S.61})$$

the Hamiltonian transforms to

$$H = \omega_b b^\dagger b + \omega_d d^\dagger d + G \cos(\omega_{EO} t) \sin \theta (b^\dagger d + b d^\dagger) + G \cos(\omega_{EO} t) \cos \theta (b^\dagger b - d^\dagger d), \quad (\text{S.62})$$

where $\omega_b = \omega_0 + \sqrt{\delta\omega^2 + J^2}$, $\omega_d = \omega_0 - \sqrt{\delta\omega^2 + J^2}$. For modulation frequency ω_m much larger than the cavity decay rates κ_b, κ_d of the supermodes b, d , the sidebands of mode b and d generated by the frequency modulated term $\Omega \cos(\omega_{EO} t) \cos \theta (b^\dagger b - d^\dagger d)$ are no longer on resonance, which can be neglected safely. Therefore, the Hamiltonian reduces to

$$H = \omega_b b^\dagger b + \omega_d d^\dagger d + G \cos(\omega_{EO} t) \sin \theta (b^\dagger d + b d^\dagger). \quad (\text{S.63})$$

If only mode m_2 couples with the waveguide with rate $\sqrt{2\kappa_{m,2}}$, mode b and d experiences effective coupling strength of $\sqrt{2\kappa_{m,2}}\cos\frac{\theta}{2}$ and $\sqrt{2\kappa_{m,2}}\sin\frac{\theta}{2}$, respectively. For the case of large detuning $\delta\omega \gg \{J, \kappa\}$, $b \approx m_1$, $d \approx m_2$, mode b is approximately decoupled from the waveguide and its lifetime is only limited by the intrinsic loss. In the rotating frame of $\omega_b b^\dagger b + \omega_d d^\dagger d$ and apply the rotating wave approximation, the Hamiltonian is

$$H = \frac{1}{2}\Omega \sin\theta \left(b^\dagger d e^{i\delta} + b d^\dagger e^{-i\delta} \right), \quad (\text{S.64})$$

where $\delta = \omega_d - (\omega_b - \omega_d)$. Transforming the Hamiltonian further to the frame of $\frac{\delta}{2}c^\dagger c - \frac{\delta}{2}d^\dagger d$, we obtain the time-independent form

$$H = -\frac{\delta}{2}b^\dagger b + \frac{\delta}{2}d^\dagger d + \frac{1}{2}G \sin\theta (b^\dagger d + b d^\dagger). \quad (\text{S.65})$$

In this way, we obtain the coupling between mode b (m_1) in the artificial atom cavity and the mode d (m_2) in the antenna cavity. The frequency difference between mode d and b is compensated by the frequency of the EO drive. For input photon with pulse shape $A_{in}(t)$, it is rapidly coupled into the antenna cavity due to the large waveguide-cavity coupling rate and then coupled to the artificial atom by a time-dependent $G(t)$. For two incident photons with the same frequency, we use different ω_{EO} to couple them with energy levels of different frequencies without crosstalk.

B. Quantum storage of control photon pulse

We use the photonic molecule introduced in the last section for the storage and readout of the control photon from the waveguide to the artificial atom. The total Hamiltonian of the system is

$$H = \sum_j \omega_j j^\dagger j + g_{nd} a b c^\dagger + \Omega(t) b d^\dagger + h.c. \quad (\text{S.66})$$

where $j \in \{a, b\}$ represents the mode in the atomic cavity in the fundamental frequency band, c is the mode in the atomic cavity in the SH frequency band, d is the mode in the antenna cavity. The dynamics of the cavity field operator A follow

$$\frac{d}{dt}A = -i[A, H] - \kappa_A A + \sqrt{2\kappa_{A,1}}A_{in}(t). \quad (\text{S.67})$$

The information of the pulse shape is contained in the time dependent term $A_{in}(t)$.

Here, we investigate the quantum storage of single photon with the photonic molecule. Without the control photon, the strong $\chi^{(2)}$ interaction is forbidden, the Hamiltonian for photon storage is

$$H = \delta_b b^\dagger b + \delta_d d^\dagger d + \Omega b^\dagger d + \Omega^* b d^\dagger. \quad (\text{S.68})$$

For single-photon excitation, the state can be described by a pure state with a general form of the superposition of Fock states. The single-photon state is expressed as

$$|\psi\rangle_{db} = c_{10}|10\rangle + c_{01}|01\rangle, \quad (\text{S.69})$$

where $|mn\rangle = |m\rangle_d \otimes |n\rangle_b$. The dynamics follows

$$\begin{aligned} \frac{d}{dt}c_{mn} &= \frac{d}{dt}\langle mn|\psi\rangle \\ &= \langle mn|\frac{d}{dt}\psi\rangle \\ &= -i\langle mn|H_{\text{eff}}|\psi\rangle \\ &= (-i\delta_b - \kappa_b) \sum_{m'n'} c_{m'n'} \langle mn|b^\dagger b|m'n'\rangle + (-i\delta_d - \kappa_d) \sum_{m'n'} c_{m'n'} \langle mn|d^\dagger d|m'n'\rangle \\ &\quad -i \left(\Omega \sum_{m'n'} c_{m'n'} \langle mn|b^\dagger d|m'n'\rangle + \Omega^* \sum_{m'n'} c_{m'n'} \langle mn|b d^\dagger|m'n'\rangle \right) \\ &= \alpha_b n c_{mn} + \alpha_d m c_{mn} - i\Omega \sqrt{(m+1)n} c_{m+1,n-1} - i\Omega^* \sqrt{m(n+1)} c_{m-1,n+1}, \end{aligned} \quad (\text{S.70})$$

where $\alpha_i = -i\delta_i - \kappa_i$, H_{eff} is the effective Hamiltonian that includes the mode dissipation, which is obtained by replacing δ_i by α_i in Eq. S.68. Under single-photon pulse excitation of a perfectly phase-matched cavity $\alpha_i = \kappa_i$, the dynamics of the intracavity and output fields follow

$$\frac{d}{dt}c_{10} = -\kappa_d c_{10} - i\Omega^*(t)c_{01} + \sqrt{2\kappa_{d,1}}\phi_{in}(t), \quad (\text{S.71})$$

$$\frac{d}{dt}c_{01} = -\kappa_b c_{01} - i\Omega(t)c_{10}, \quad (\text{S.72})$$

$$\phi_{out} = \phi_{in} - \sqrt{2\kappa_{c,1}}c_{10}, \quad (\text{S.73})$$

where $\phi_{in}(t)$ ($\phi_{out}(t)$) represents the pulse shape of the input (output) single photon.

1. Figure of merit

We assume that both cavities are in the ground state, so $c_{10} = c_{01} = 0$ at $t = 0$. We also assume that the input field excitation $\phi_{in}(t)$ only has nonzero values in time interval $[0, T]$. Our goal is to store the input field to $|01\rangle$ and retrieve the photon out of the cavity after. During the storage process, $c_{10}(0) = c_{01}(0) = 0$ and the input field fulfills $\int_0^T dt |\phi_{in}(t)|^2 = 1$. The storage efficiency is given by

$$\begin{aligned} \eta_s &= \frac{\text{Population of } |01\rangle}{\text{Number of incoming photons}} \\ &= |c_{01}(T)|^2. \end{aligned} \quad (\text{S.74})$$

For the retrieval process, we set $c_{10}(t_r) = 0$, $c_{01}(t_r) = 1$ with t_r being the start time of the retrieve. The retrieval efficiency is given by

$$\begin{aligned} \eta_r &= \frac{\text{Number of retrieved photons}}{\text{Population of } |01\rangle} \\ &= \int_{t_r}^{\infty} |\phi_{out}(t)|^2 dt. \end{aligned} \quad (\text{S.75})$$

2. Photon Retrieval

First, we investigate the retrieval process with $\phi_{in}(t) = 0$ for $t > t_r$. In our case, we have assumed that the second cavity has a quality factor much larger than the first one which couples with a bus waveguide, thus it is reasonable to make a approximation $\kappa_b \approx 0$. From Eqs. (S.71)-(S.72),

$$\frac{d}{dt}(|c_{10}|^2 + |c_{01}|^2) = -2\kappa_d |c_{10}|^2. \quad (\text{S.76})$$

Using Eq. (S.73) and Eq. (S.75), the retrieval efficiency is derived as

$$\begin{aligned} \eta_s &= 2\kappa_{d,1} \int_{t_r}^{\infty} dt |c_{10}|^2 \\ &= -\frac{\kappa_{d,1}}{\kappa_d} \int_{t_r}^{\infty} dt \frac{d}{dt} (|c_{10}|^2 + |c_{01}|^2) \\ &= \frac{\kappa_{d,1}}{\kappa_{d,0} + \kappa_{d,1}} (|c_{10}(t_r)|^2 + |c_{01}(t_r)|^2 - |c_{10}(\infty)|^2 - |c_{01}(\infty)|^2). \end{aligned} \quad (\text{S.77})$$

If there is no excitation in the cavity after the retrieval process, $|c_{10}(\infty)|^2 = |c_{01}(\infty)|^2 = 0$, the efficiency reduces to

$$\eta_s = \frac{\kappa_{d,1}}{\kappa_{d,0} + \kappa_{d,1}}. \quad (\text{S.78})$$

Therefore, the retrieval efficiency is independent of the pulse shape of the driving fields, provided that the driving field pumps all excitation out of the cavity completely. To achieve high retrieval efficiency, over-coupled condition of the waveguide-cavity system is required.

In the following, we derive the relationship between the pulse shapes of the driving field and the output field. For adiabatic retrieval process, the input and driving fields are smooth. It is reasonable to adiabatically eliminate c_{10} , the population of state $|10\rangle$, in the coupled equations, if $\kappa_d \gg g/T$. Then Eq. (S.71) transforms to

$$-\kappa_d c_{10} - i\Omega c_{01} = 0. \quad (\text{S.79})$$

Combining it with Eq. (S.72), we get

$$\frac{d}{dt} c_{01} = -\frac{|\Omega(t)|^2}{\kappa_d} c_{01}. \quad (\text{S.80})$$

Solving this differential equation and using the boundary condition $c_{01}(0) = 1$ (the start time of the retrieval process is set to be 0 for simplicity),

$$c_{01}(t) = e^{-\frac{1}{\kappa_d} \int_0^t |g(t')|^2 dt'}. \quad (\text{S.81})$$

Denote $h(t, t') = \int_t^{t'} |\Omega(t'')|^2 dt''$ and submit it into Eq. (S.73), the output field is derived as

$$\phi_{out}(t) = i \frac{\sqrt{2\kappa_{d,1}}}{\kappa_d} \Omega(t) e^{-\frac{1}{\kappa_d} h(0,t)}. \quad (\text{S.82})$$

Computing the retrieval efficiency using Eq. (S.82),

$$\begin{aligned} \eta_r &= \int_0^\infty dt |\phi_{out}|^2 \\ &= \frac{2\kappa_{d,1}}{\kappa_d^2} \int_0^\infty dt |\Omega(t)|^2 e^{-\frac{2}{\kappa_d} \int_0^t dt' |g(t')|^2} \\ &= \frac{\kappa_{d,1}}{\kappa_d} \left(e^{-\frac{2}{\kappa_d} h(0,0)} - e^{-\frac{2}{\kappa_d} h(0,\infty)} \right) \\ &= \frac{\kappa_{d,1}}{\kappa_{d,0} + \kappa_{d,1}} \left(1 - e^{-\frac{2}{\kappa_d} h(0,\infty)} \right). \end{aligned} \quad (\text{S.83})$$

For strong or long driving pulse, $h(0, \infty) \gg 1$, the retrieval efficiency reduces to the previously derived form $\frac{\kappa_{d,1}}{\kappa_{d,0} + \kappa_{d,1}}$.

To be more practical, we consider the case that not all excitation are driven out of the cavity, which means either $c_{01}(\infty)$ or $c_{10}(\infty)$ does not equal to zero. The efficiency can be obtained by giving $h(0, \infty)$ a finite value. Here, we shape the driving field $\Omega(t)$ to retrieve the photon to the desired mode $A_{in}(t)$ (the input shape). Equaling $\sqrt{\frac{\kappa_{d,1}}{\kappa_{d,0} + \kappa_{d,1}}} A_{in}(t)$ and eq. S.82 and their norm square integrals,

$$\sqrt{\frac{\kappa_{d,1}}{\kappa_{d,0} + \kappa_{d,1}}} A_{in}(t) = i \frac{\sqrt{2\kappa_{d,1}}}{\kappa_d} \Omega(t) e^{-\frac{1}{\kappa_d} h(0,t)}, \quad (\text{S.84})$$

so

$$\int_0^t dt' |A_{in}(t)|^2 = 1 - e^{-\frac{2}{\kappa_d} h(0,t)}. \quad (\text{S.85})$$

We derive the optimal retrieval pulse shape

$$\begin{aligned} \Omega(t) &= -i \sqrt{\frac{\kappa_d}{2}} e^{h(0,t)/\kappa_c} A_{in}(t) \\ &= -i \sqrt{\frac{\kappa_d}{2}} \frac{A_{in}(t)}{\sqrt{\int_t^\infty dt' |A_{in}(t')|^2}}. \end{aligned} \quad (\text{S.86})$$

For photon storage, it is the time reverse of the retrieve process [51]. One can use driving pulse $\Omega^*(t_r - t)$ to store input pulse of shape $A_{in}(t)$ with maximal efficiency.

C. Transmission of the target photon

The target photon ($a_{in}(t)$) can also be coupled to the artificial atom mediated by the antenna under an EO drive. However, when the two modes a and b in the artificial atom are designed to fulfill phase-match condition with mode c , whether the target photon can enter into mode b of the artificial atom ($|1_a 1_b\rangle$) strongly depends on the quantum state of mode a . For sufficiently large nonlinear coupling strength g_{nd} , the degeneracy of two-excitation states $|1_a 1_b 0_c\rangle$ and $|0_a 0_b 1_c\rangle$ will be removed, resulting in two new eigenstates with the form of superposition of $|1_a 1_b 0_c\rangle$ and $|0_a 0_b 1_c\rangle$ and eigenenergies split by $2g_{nd}$. The sum of the two photon frequencies no longer equals to the resonant frequency of two-excitation states. If the control photon has already been stored into mode b , the target photon is no longer resonant with the transition from $|0_a 1_b 0_c\rangle$ to $|1_a 1_b 0_c\rangle$, thus will be blocked. Accordingly, the phase of the target photon is controlled by the state of the stored control photon in the artificial atom.

In this work, we take the artificial atom based on non-degenerate three-wave mixing for constructing quantum phase gate, thus the total system Hamiltonian is

$$H = \omega_d d^\dagger d + \omega_a a^\dagger a + \omega_b b^\dagger b + \delta_c c^\dagger c + \Omega a^\dagger d + g_{nd} abc^\dagger + h.c. \quad (S.87)$$

For EO driving strength $\kappa_A \ll \Omega \ll g_{nd}$, the waveguide is effectively over-coupled with the atom. The target photon couples into and out from the atom for the control photon in state $|0\rangle$, whereas transmit directly without entering the atom for control photon in state $|1\rangle$. In this case, it is no longer necessary to design the shape of the EO drive, but requires carefully choosing an appropriate strength.

In the two-excitation subspace, the state can be described by a pure state with a general form of the superposition of Fock states. For mode a in state $|1\rangle$ and very long lifetime, the single-photon state is expressed as

$$|\psi\rangle_{dbac} = c_{1010}|1010\rangle + c_{0110}|0110\rangle + c_{0001}|0001\rangle, \quad (S.88)$$

where $|mnkl\rangle = |m\rangle_d \otimes |n\rangle_a \otimes |k\rangle_b \otimes |l\rangle_c$. The dynamics follows

$$\begin{aligned} \frac{d}{dt}c_{mnkl} &= \frac{d}{dt}\langle mnkl|\psi\rangle \\ &= \langle mnkl|\frac{d}{dt}\psi\rangle \\ &= -i\langle mnkl|H_{eff}|\psi\rangle \\ &= \alpha_d \sum_{m'n'k'l'} c_{m'n'k'l'} \langle mnkl|d^\dagger d|m'n'k'l'\rangle + \alpha_b \sum_{m'n'k'l'} c_{m'n'k'l'} \langle mnkl|b^\dagger b|m'n'k'l'\rangle \\ &\quad + \alpha_a \sum_{m'n'k'l'} c_{m'n'k'l'} \langle mnkl|a^\dagger a|m'n'k'l'\rangle + \alpha_c \sum_{m'n'k'l'} c_{m'n'k'l'} \langle mnkl|c^\dagger c|m'n'k'l'\rangle \\ &\quad - i\Omega \left(\sum_{m'n'k'l'} c_{m'n'k'l'} \langle mnkl|a^\dagger d|m'n'k'l'\rangle + \sum_{m'n'k'l'} c_{m'n'k'l'} \langle mnkl|ad^\dagger|m'n'k'l'\rangle \right) \\ &\quad - ig_{nd} \left(\sum_{m'n'k'l'} c_{m'n'k'l'} \langle mnkl|a^\dagger b^\dagger c|m'n'k'l'\rangle + \sum_{m'n'k'l'} c_{m'n'k'l'} \langle mnkl|abc^\dagger|m'n'k'l'\rangle \right) \\ &= \alpha_d m c_{mnkl} + \alpha_a n c_{mnkl} + \alpha_b k c_{mnkl} + \alpha_c l c_{mnkl} \\ &\quad - i\Omega \sqrt{m(n+1)} c_{(m-1)(n+1)kl} - i\Omega \sqrt{(m+1)n} c_{(m+1)(n-1)kl} \\ &\quad - ig_{nd} \sqrt{nk(l+1)} c_{m(n-1)(k-1)(l+1)} - ig_{nd} \sqrt{(n+1)(k+1)l} c_{m(n+1)(k+1)(l-1)}. \end{aligned} \quad (S.89)$$

For our two-photon case

$$\frac{d}{dt}c_{1010} = \alpha_d c_{1010} + \alpha_b c_{1010} - i\Omega c_{0110} - i\phi_{in}(t), \quad (S.90)$$

$$\frac{d}{dt}c_{0110} = \alpha_b c_{0110} + \alpha_a c_{0110} - i\Omega c_{1010} - ig_{nd} c_{0001}, \quad (S.91)$$

$$\frac{d}{dt}c_{0001} = \alpha_c c_{0001} - ig_{nd} c_{0110}. \quad (S.92)$$

The dynamics of the system depends on the initial state of the system. Initially, we set $c_{1010} = c_{0110} = c_{0001} = 0$ to solve the dynamics of the system.